







# Cholesterol-containing lipid nanodiscs promote an $\alpha$ -synuclein binding mode that accelerates oligomerization

Martin Jakubec<sup>1,2</sup> , Espen Bariås<sup>1,2</sup>, Samuel Furse<sup>2</sup> , Morten L. Govasli<sup>1,2,3</sup> , Vinnit George<sup>4</sup>, Diana Turcu<sup>1,2</sup>, Igor A. Iashchishyn<sup>5</sup> , Ludmilla A. Morozova-Roche<sup>5</sup>  and Øyvind Halskau<sup>1,2</sup> 

- 1 Department of Biological Sciences, University of Bergen, Norway
- 2 Department of Molecular Biology, University of Bergen, Norway
- 3 Division of Infection and Immunity, University College London, London, UK
- 4 Department of Chemistry, University of Bergen, Norway
- 5 Department of Medical Biochemistry and Biophysics, Umeå University, Sweden

## Keywords

amyloid oligomerization; cholesterol; fibrillation; lipid nanodiscs; solution-state NMR

## Correspondence

Ø. Halskau, Department of Biological Sciences, University of Bergen, PB 7803, Bergen N-5020, Norway  
Tel: +47 55584563  
E-mail: oyvind.halskau@uib.no

(Received 3 November 2019, revised 28 July 2020, accepted 1 September 2020)

doi:10.1111/febs.15551

Dysregulation of the biosynthesis of cholesterol and other lipids has been implicated in many neurological diseases, including Parkinson's disease. Misfolding of  $\alpha$ -synuclein ( $\alpha$ -Syn), the main actor in Parkinson's disease, is associated with changes in a lipid environment. However, the exact molecular mechanisms underlying cholesterol effect on  $\alpha$ -Syn binding to lipids as well as  $\alpha$ -Syn oligomerization and fibrillation remain elusive, as does the relative importance of cholesterol compared to other factors. We probed the interactions and fibrillation behaviour of  $\alpha$ -Syn using styrene-maleic acid nanodiscs, containing zwitterionic and anionic lipid model systems with and without cholesterol. Surface plasmon resonance and thioflavin T fluorescence assays were employed to monitor  $\alpha$ -Syn binding, as well as fibrillation in the absence and presence of membrane models.  $^1\text{H}$ - $^{15}\text{N}$ -correlated NMR was used to monitor the fold of  $\alpha$ -Syn in response to nanodisc binding, determining individual residue apparent affinities for the nanodisc-contained bilayers. The addition of cholesterol inhibited  $\alpha$ -Syn interaction with lipid bilayers and, however, significantly promoted  $\alpha$ -Syn fibrillation, with a more than a 20-fold reduction of lag times before fibrillation onset. When  $\alpha$ -Syn bilayer interactions were analysed at an individual residue level by solution-state NMR, we observed two different effects of cholesterol. In nanodiscs made of DOPC, the addition of cholesterol modulated the NAC part of  $\alpha$ -Syn, leading to stronger interaction of this region with the lipid bilayer. In contrast, in the nanodiscs comprising DOPC, DOPE and DOPG, the NAC part was mostly unaffected by the presence of cholesterol, while the binding of the N and the C termini was both inhibited.

## Abbreviations

AD, Alzheimer's disease; AFM, atomic force microscopy; DOPC, 1,2-dioleoyl-sn-glycero-3-phosphocholine; DOPE, 1,2-dioleoyl-sn-glycero-3-phosphoethanolamine; DOPG, 1,2-dioleoyl-sn-glycero-3-phospho-(1'-rac-glycerol); DOSY, diffusion-ordered spectroscopy; NAC, nonamyloid component; NMR, nuclear magnetic resonance; PD, Parkinson's disease; PM, plasma membrane; SMA, styrene-maleic acid; SPR, surface plasmon resonance; ThT, thioflavin T; TPE-TPP, tetraphenylethene tethered with triphenylphosphonium;  $\alpha$ -Syn,  $\alpha$ -synuclein.

## Introduction

Parkinson's disease (PD) is a protein misfolding disease associated with a conversion of  $\alpha$ -Syn from its soluble state into fibrillar aggregates. During this conversion,  $\alpha$ -Syn forms soluble, toxic oligomers that are implicated in the dopaminergic neuron cell death associated with clinical manifestations of PD [1]. The exact function of native  $\alpha$ -Syn is not fully understood, nor are the driving forces governing its misfolding, oligomerization and fibrillation, including the specific roles of individual residues within the protein. It has been proposed that  $\alpha$ -Syn plays a role in synaptic plasticity allowing 'kiss-and-run' neurotransmitter release, where the protein assists vesicles containing the neurotransmitters to fuse with the synaptic membrane transiently so that it can deliver its cargo before disengaging [2]. Unfortunately, the role of the interaction between  $\alpha$ -Syn and lipid bilayers is unclear as a consistent pattern of behaviour has not been observed (review [3]). Research, including relatively recent and comprehensive work by Viennet *et al.* [4], indicates that two important membrane general characteristics are affecting the interaction between  $\alpha$ -Syn and lipid membrane: its net charge and physical state. A higher abundance of anionic lipids, such as phosphatidylserine (PS) or phosphatidylglycerol (PG), leads to a higher affinity of  $\alpha$ -Syn and a slower aggregation [4,5]. Likewise, pronounced membrane curvature and smaller lipid head group size seem to promote the interaction of  $\alpha$ -Syn [4,6,7]. Protein modifications may also be an important factor in the PD pathology through its relationship between  $\alpha$ -Syn and the membrane [8]; acetylation at the N-terminal promotes binding while leaving aggregation behaviour largely unchanged [4,9,10]. With this in mind, there is a notable lack of knowledge regarding how cholesterol, the most abundant mammalian component of the plasma membrane (PM), affects  $\alpha$ -Syn.

Cholesterol constitutes about 50% of the mass of PMs in mammals and has a considerable effect on its physical properties, including its fluidity and permeability [11,12]. When residing in the bilayer, cholesterol is only marginally accessible to the solvent or peripheral protein interaction as it is primarily its -OH group that is exposed [13]. However, cholesterol has prominent effects on how other lipids are organized, and may in this way confer larger effects than its small exposure would initially suggest. Cholesterol is particularly abundant in the brain, and its dysregulation has been linked to several neurodegenerative diseases, including Alzheimer's disease (AD) [14,15], Huntington's disease [16] and Niemann-Pick disease type C

[17,18]. Recent evidence suggests that cholesterol is more abundant in the inner monolayer of the synaptic membrane, where  $\alpha$ -Syn makes contact with the PM as part of its function [19]. It has also been observed that the cholesterol abundance in the PM of neurons decreases with age, which in turn could drive or confer vulnerability towards neurodegeneration [20]. This age-dependent loss of cholesterol from the PM seems to affect the release of neurotransmitters by hindering the fusion of presynaptic vesicles [21]. However, the clinical connection between PD and cholesterol abundance and distribution remains unclear. There is evidence that higher level of serum cholesterol is associated with a higher risk of PD [22] and a decrease in the risk of PD [23], or is not associated with PD at all [3,24].

There are also contradictory results regarding the interaction of  $\alpha$ -Syn and cholesterol at the molecular level. A cholesterol-binding site in the nonamyloid component (NAC) of  $\alpha$ -Syn has been reported, and that through this site, cholesterol is essential for the formation of cytotoxic 'amyloid pores' [25–27]. However, recent work has shown that the presence of cholesterol inhibits the binding of  $\alpha$ -Syn to membranes comprising either zwitterionic or anionic lipids [28,29]. The apparent discrepancy in affinity between  $\alpha$ -Syn and cholesterol, and the interaction of  $\alpha$ -Syn and lipid head groups have, to our knowledge, not been explained adequately. Despite contradictory and incomplete evidence, current knowledge strongly suggests a role for cholesterol in both the normal function and misfolding of  $\alpha$ -Syn.

The investigation of reversible protein–membrane interactions often relies on lipid vesicles or supported lipid bilayers [30]. However, such lipid assemblies limit the interpretation and application of many methods including solution-state NMR, steady-state affinity measurements and fibrillation studies [31]. Nanodiscs, consisting of circular patches of lipid bilayer surrounded by a polymer belt, have emerged as an alternative to vesicles and have been successfully used in structural studies of membrane proteins and anchored peripheral proteins [31,32]. As they can be prepared with narrow size distributions, well-defined lipid compositions and are stable in solution, they are promising tools for studying reversible protein–lipid interactions [32,33]. In this study, we use styrene–maleic acid (SMA) nanodiscs as the primary membrane model system for our studies. These nanodiscs have properties similar to those that are prepared using a protein belt to scaffold the lipids, but allow detergent-free sequestration of lipids directly from a vesicle or even native membranes [32]. Recently, protein-scaffolded nanodiscs were used to investigate the role of charge and

fluidity on  $\alpha$ -Syn binding and aggregation [4]. The study notes that while high-resolution solution-state NMR is made possible by nanodiscs and yields sequence-specific binding information, it does not allow direct detection of  $\alpha$ -Syn membrane-bound state [4]. However, their comprehensive work allowed them to propose a model for  $\alpha$ -Syn membrane interaction and its effect on fibrillation that focused on the protein competing for favourable binding sites on fluid patches with net negative charge. In their model, increased fibrillation occurred when  $\alpha$ -Syn competed for the most favourable binding sites, bringing exposed NAC regions together [4]. Given the importance of cholesterol for  $\alpha$ -Syn binding and the implication of the NAC region, further detailed investigation focusing on the effect of cholesterol is warranted.

We hypothesize that there is an interplay between cholesterol abundance of the membrane and the reversible and dynamic  $\alpha$ -Syn binding, the protein conformational response, and ultimately the protein oligomerization and fibrillation outcome. We further propose that the changes in the protein conformation are primarily driven by an interaction between the NAC region and cholesterol-induced ordering of the bilayer. We present a comparative lipid-dependent binding and fibrillation study of recombinant  $\alpha$ -Syn using SMA lipid nanodiscs consisting of zwitterionic DOPC and a membrane model containing DOPC, PE and PG in a 4 : 3 : 1 ratio. Each model was also prepared with 30% (w/w) cholesterol. As an indicator for how the presence of nanodiscs affects  $\alpha$ -Syn at a detailed level, we have determined residue-specific apparent binding constants for ~40% of residues evenly distributed within the  $\alpha$ -Syn sequence using increasing widths of  $^1\text{H}$ - $^{15}\text{N}$  HSQC cross-peaks and formalism adapted from Shortridge *et al.* [34]. Lastly, we monitored the effect of cholesterol in lipid nanodiscs on oligomerization rates of  $\alpha$ -Syn by using thioflavin T (ThT) and a novel tetraphenylethene tethered with triphenylphosphonium (TPE-TPP) fluorescence marker [35], potentially allowing earlier detection of the onset of fibrillation than the standard ThT approach.

## Results

### Binding of $\alpha$ -Syn monomers to lipid vesicles is inhibited by cholesterol

Vesicles systems are the material basis for SMA nanodiscs [32] and are commonly used membrane model systems in their own right. A zwitterionic vesicle model with a mean diameter of ~100 nm was prepared using

DOPC alone, as well as a more complex anionic model using DOPC : PE : PG in a 4 : 3 : 1 molar ratio. The structures of lipids used and a representative vesicle diameter distribution, as determined by DLS, are shown in Fig. S1. Each model was also prepared with 30% (w/w) cholesterol, yielding a total of four different lipid compositions. Representative surface plasmon resonance (SPR) plots of  $\alpha$ -Syn binding to these lipid models in room temperature are shown in Fig. 1A–D. The steady-state dissociation equilibrium constants,  $K_D$ , of  $\alpha$ -Syn were estimated using Eqn (1) (Fig. 1D). The dissociation constant for DOPC mixtures was approximately 7.2 times higher ( $1072 \pm 137$  nm) than that for DOPC : PE : PG vesicles ( $148 \pm 36$  nm) [36–39]. Vesicles containing 30% (w/w) cholesterol showed an almost twofold increase in the  $K_D$  ( $2138 \pm 322$  nm for DOPC and  $273 \pm 36$  nm for DOPC : PE : PG vesicles). These values indicate that cholesterol addition to these overall fluid systems has a general inhibitory effect on binding, as the  $K_D$  was increased in both lipid models. We then wanted to explore how this observation translated into changes in  $\alpha$ -Syn fold and aggregation behaviour. However, the bulky and quasi-stable vesicle models are not suitable for fibrillation studies that often span days [40], and the use of vesicles is not suitable for NMR studies directly monitoring individual residues [41].

### Preparation and characterization of SMA nanodiscs

We therefore prepared nanodiscs from 100-nm vesicles of the same compositions as used for the SPR affinity measures. This was done by adding SMA to 1% w/v and overnight incubation followed by size-exclusion chromatography (SEC) purification. Although the presence of cholesterol and PE in the vesicles inhibited proper nanodisc formation, we were able to optimize the process as described in Fig. 2A,B, Tables S1, S2 and Fig. S1. Nanodisc zeta potential and dimensions as determined by DLS are summarized in Fig. 2A,B. Inclusion of cholesterol into the nanodiscs was verified using LC-MS/MS (Fig. S3).

Given the importance of phase behaviour in  $\alpha$ -Syn interaction and aggregation behaviour [4,9,37], we also investigated the nanodiscs and vesicles comparatively using laurdan, a lipid-sensitive fluorescence probe. Laurdan is a fluorescent reporter molecule that locates itself at the hydrophobic–hydrophilic interface of a membrane and enables investigators to indirectly observe lipid packing, a property that is relatable to fluidity [42,43]. Both laurdan excitation and emission spectra are affected by the polarity of the surrounding

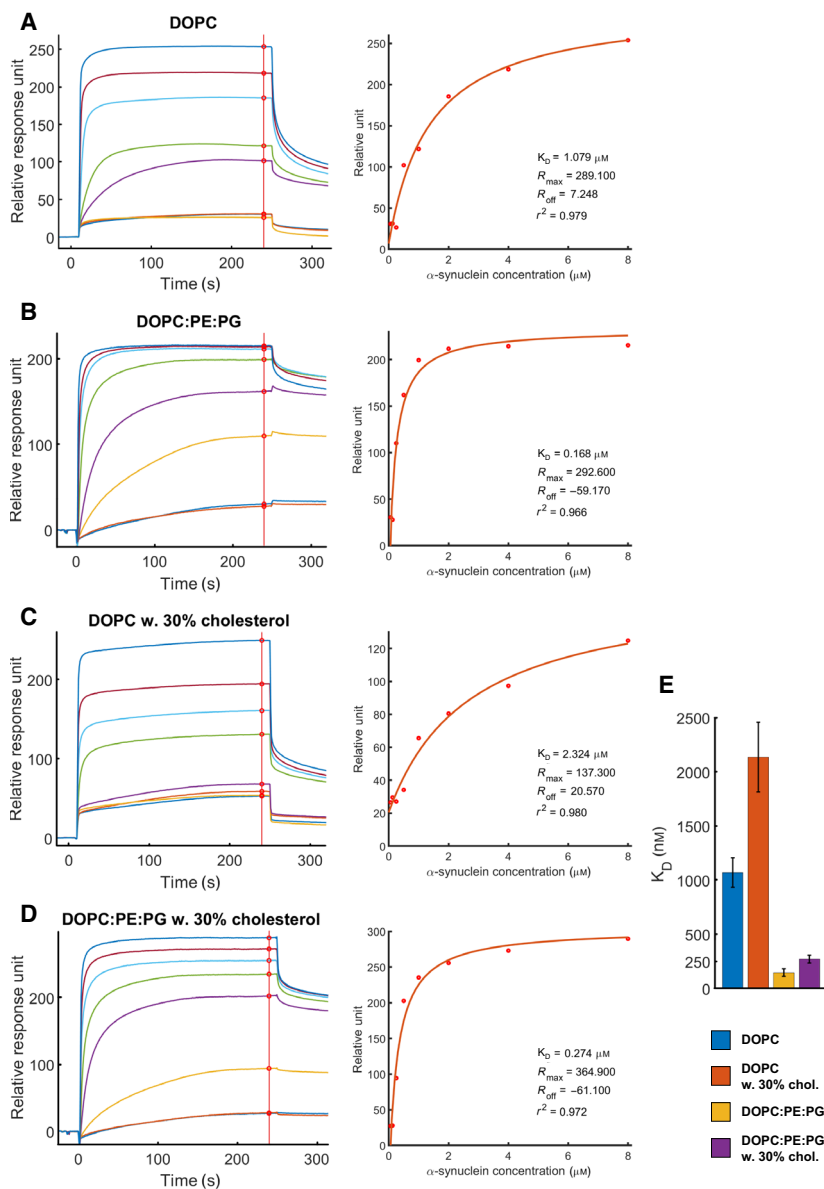


**Fig. 1.** Monomeric  $\alpha$ -Syn binding to vesicles is inhibited by cholesterol. Representative SPR plots of  $\alpha$ -Syn interaction with immobilized lipid layers of DOPC (A) and mixtures of DOPC : PE : PG (4 : 3 : 1) (B), without and with the addition of 30% (w/w) cholesterol (C and D, respectively). Equilibrium values are indicated with red circles where the vertical lines intersect the sensorgrams. Red line represents fitting into Eqn (1). (E) Mean  $K_D$  values for each lipid group. Each value represents 3–5 replicates, and error bars depict standard deviations.

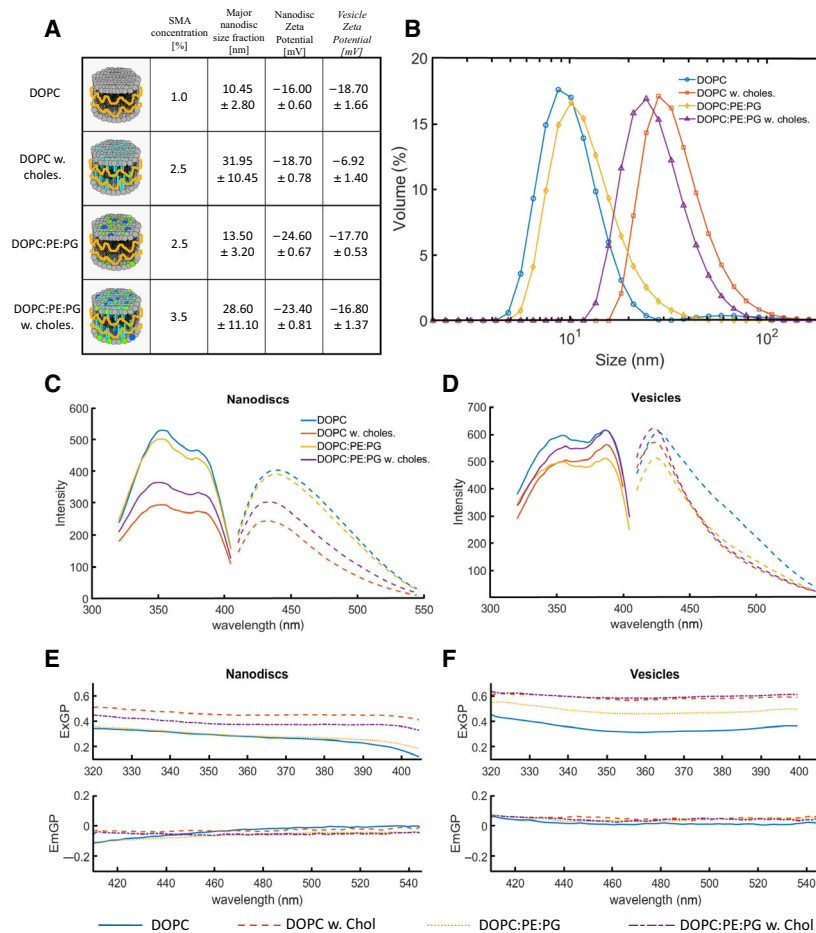
environment and by the water dipolar relaxation [44,45]. Excitation spectra (Fig. 2C,D) for both lipid nanodiscs and lipid vesicles contain two peaks, at 350 and 390 nm. The peak at 350 nm reports on the liquid crystalline phase of the lipid bilayer, while the peak at 390 nm indicates a denser packing of lipids around laurdan and is associated with the presence of a gel phase. Overall, however, the results show that our bilayers are predominantly fluid in the absence of cholesterol. This is also confirmed by the calculated generalized polarization functions, where a low ExGP and the presence of a negative slope as the wavelength increases are indicative of a fluid phase (Fig. 2E,F) [46,47]. Upon addition of cholesterol, there is an

increase in the overall ExGP function in all cases, indicating an ordering of the bilayer. This response is not as large for nanodiscs, however, suggesting that these lipids remain more solvent-accessible than their vesicle counterparts.

### The presence of cholesterol in the lipid nanodiscs influences both lag time and rate of fibrillation of $\alpha$ -Syn

We then used the lipid nanodiscs to explore how the different bilayer models affected the fibrillation rate of  $\alpha$ -Syn. ThT and TPE-TPP fluorescence assays were used to measure the fibrillation of  $\alpha$ -Syn both in the

**Fig. 2.** Nanodiscs preparation and characterization. (A) Table of lipid nanodiscs' physical properties. Four compositions of nanodiscs have been used: DOPC, DOPC with 30% (w/w) cholesterol, DOPC : PE : PG (4 : 3 : 1) and DOPC : PE : PG with 30% (w/w) cholesterol. Size and zeta potential were measured using Nanosizer ZS. (B) DLS measurement of prepared nanodiscs which were purified by SEC. Both DOPC and DOPC : PE : PG (4 : 3 : 1) nanodiscs without cholesterol are smaller (mean sizes: 10 and 13 nm, respectively) than nanodiscs containing 30% (w/w) cholesterol (32 and 29 nm, respectively). (C, D) Laurdan excitation and emission spectra for lipid nanodiscs and vesicles at 37 °C. Excitation spectra (full line) were collected using a fixed emission wavelength of 430 nm. Emission spectra (dashed line) were collected using a fixed excitation wavelength of 390 nm. (E, F) Laurdan excitation (ExGP) and emission (EmGP) generalized polarization functions for lipid nanodiscs and vesicles in 37 °C, calculated using Eqns (S1) and (S2), respectively, from Bagatolli *et al.* [46].



absence and in the presence of lipid nanodiscs at 37 °C. ThT is a fluorescence probe that is widely used to characterize the aggregation of various amyloidogenic peptides, also in the presence of lipid bilayers [48–50]. In contrast, TPE-TPP is, to our knowledge, untested as a fluorescence marker in the presence of lipids. The compound is a structural ThT analogue developed by Leung *et al.* [35]. It binds to fibrils by a similar mechanism as ThT, but it is two orders of magnitude more sensitive and therefore potentially an earlier reporter of fibrillation [51].

We adopted a high-throughput technique, using 384-well plates and incubation time of up to 150 h [52]. Briefly, we evaluated the experiment using cumulative curve plots, where each well is annotated as either positive or negative based on its fluorescence signal [52]. The percentage of positive wells against time is then plotted (Fig. 3A), and from this, the lag time for each experimental condition can be read directly. The lag time of  $\alpha$ -Syn, 20 h, increased in the presence of DOPC and DOPC : PE : PG lipid

nanodiscs to 50 and 60 h, respectively. However, with cholesterol present in the lipid nanodiscs, the lag time dropped to 3 and 2 h, respectively. We then evaluated the experiment more in-depth, by fitting the fluorescence signals from each well independently to a two-step Finke–Watzky model [53] (Eqn 2). From this model, we obtained the  $t_N$  (lag time, Eqn 3) and  $\nu$  (fibrillation rate). The ratio of  $t_N/t_{N \text{ control}}$  and  $\nu/\nu_{\text{control}}$  is presented in Fig. 3B,C.

Using the TPE-TPP fluorescence dye, we were able to detect the early stages of fibrillation of  $\alpha$ -Syn alone (Fig. S4B). However, with the addition of lipid nanodiscs we observed a loss of fluorescence (Fig. S5). This suggests the release of TPE-TPP from the cross- $\beta$ -sheets of  $\alpha$ -Syn and its interaction with the lipid nanodiscs. TPE-TPP was therefore deemed unsuitable for fibrillation studies in the presence of our model system of choice, but did serve well as an early and sensitive marker for fibrillation events. The results presented below are therefore derived from ThT-based assays only.



The  $t_N$  ratio (lag time ratio) is three times higher when nanodiscs (without cholesterol) are present during fibrillation ( $3.1 \pm 0.77$  for  $\alpha$ -Syn and DOPC,  $3.5 \pm 0.84$  for  $\alpha$ -Syn and DOPC : PE : PG and  $1.0 \pm 0.38$  for  $\alpha$ -Syn alone,  $t$ -test  $P < 0.01$ ). However, the fibrillation rate ratio,  $\nu$ , did not change significantly ( $1.0 \pm 0.22$  for  $\alpha$ -Syn alone,  $0.7 \pm 0.22$  for  $\alpha$ -Syn and DOPC, and  $1.0 \pm 0.05$  for  $\alpha$ -Syn and DOPC : PE : PG). When cholesterol was present, the  $t_N$  ratio approached zero as the fluorescence started to increase almost immediately after the addition of lipid nanodiscs ( $-0.01 \pm 0.20$  for  $\alpha$ -Syn and DOPC with 30% cholesterol and  $-0.03 \pm 0.03$  for  $\alpha$ -Syn and DOPC : PE : PG with 30% cholesterol). Moreover, we observed a significant 14-fold increase in the  $\nu$  ratio in the presence of cholesterol compared to the control ( $15 \pm 2.26$  for  $\alpha$ -Syn and DOPC with 30% cholesterol and  $13 \pm 2.13$  for  $\alpha$ -Syn and DOPC : PE : PG with 30% cholesterol,  $t$ -test,  $P \ll 0.01$ ).

We also monitored the morphology of  $\alpha$ -Syn during the lag phase of fibrillation kinetics using atomic force microscopy (AFM) (Fig. 3D). For  $\alpha$ -Syn incubated alone, we did not find any fibrils, and only small granular deposits of  $\alpha$ -Syn were observed by using both  $10 \times 10 \mu\text{m}$  and  $2 \times 2 \mu\text{m}$  scan sizes (Fig. 3D insets). In  $\alpha$ -Syn + DOPC sample, we can clearly observe the DOPC nanodisc as spheres of 50–100 nm, larger than the diameters in Table S1. Small deposits of  $\alpha$ -Syn alone were not visible at the background. In the  $2 \times 2 \mu\text{m}$  scan size, however, we observe what we interpret as some aggregation of  $\alpha$ -Syn around the nanodiscs. The same situation, but also with cholesterol present, shows a more diverse morphology, where nanodiscs and  $\alpha$ -Syn co-aggregate to a larger extent. The  $2 \times 2 \mu\text{m}$  scan size in the inset shows an  $\alpha$ -Syn fibril. In the case of the negatively charged DOPC : PE : PG nanodiscs with cholesterol, we observed a mix of morphologies consistent of discs with associated  $\alpha$ -Syn aggregates. The  $2 \times 2 \mu\text{m}$  inset shows fibril morphologies, although the fibrils are shorter and more diffuse than in the case of DOPC with cholesterol.

### Cholesterol affects the interaction of $\alpha$ -Syn and lipid bilayer differently in DOPC and DOPC : PE : PG lipid models

While our results clearly show that cholesterol affects both binding and aggregation behaviour of  $\alpha$ -Syn, it is unclear how the protein itself is affected by the different nanodisc membrane models. To explore the mechanism of  $\alpha$ -Syn and cholesterol interaction at a more

detailed level, we proceeded with NMR studies to determine which amino acids are affected in the presence of lipid nanodiscs. Lipid nanodiscs of the compositions described above were titrated into  $^{15}\text{N}$ -labelled  $\alpha$ -Syn, and HSQC fingerprints were acquired at 299K to monitor changes in the chemical environment of individual residues. Cross-peak assignments were adapted from BMRB entry 6968 [54] and 25227 [55] and verified using  $C_\alpha$  and  $C_\beta$  chemical shifts from standard triple-resonance experiments performed on a double-labelled  $\alpha$ -Syn sample. In agreement with other studies [56–58], we did not observe any chemical shifts of cross-peaks, which would represent a direct observation of changes in the chemical environment. Instead, we observed line (peak) broadening which grows beyond detection in the high concentrations of lipid nanodiscs (Fig. 4A). These undetectable peaks, sometimes called invisible states, are ascribed to chemical exchange broadening or efficient relaxation pathways related to molecular motions [56]. Free and lipid-associated  $\alpha$ -Syn in exchange between states, intramolecular interaction in folding and intermolecular oligomerization may all cause line broadening and loss of observable states. We evaluated these invisible states as possible binding curves, using logic presented by Shortridge *et al.* [34] for estimating protein/ligand affinity. Between 77 ( $\alpha$ -Syn and DOPC : PE : PG with 30% cholesterol) and 82 ( $\alpha$ -Syn and DOPC) cross-peaks and their individual line-broadening behaviour in response to lipid nanodiscs were observed for each lipid nanodisc model. Using the PINT software [59], we deconvoluted peaks for each assigned amino acid and calculated a residue-specific apparent  $K_D$  ( $aK_D$ ) based on Eqn (4) [34], which provides values biased towards the lower limit of the actual, unknown  $K_D$  [4]. From 48 ( $\alpha$ -Syn and DOPC : PE : PG with 30% cholesterol) to 67 ( $\alpha$ -Syn and DOPC) cross-peaks had good correlations with the model ( $r > 0.90$ , examples shown in Fig. 4B, all extracted  $aK_D$  values in Table S4B).

In order to visualize the results, each residue-specific  $aK_D$  was then plotted as a function of lipid nanodisc composition and its position in the  $\alpha$ -Syn primary sequence (Fig. 4C). High values of  $aK_D$  ( $> 500 \mu\text{M}$ ) were observed in the C-terminal part of  $\alpha$ -Syn in the presence of all lipid models. The lowest  $aK_D$  values were observed for N-terminal part of  $\alpha$ -Syn, suggesting that this part of the molecule is essential for the binding to lipid bilayers. This is consistent with earlier studies [4,60,61]. Overall, the heatmap suggests that there are three distinct regions of  $\alpha$ -Syn: the N-terminal with high affinity for lipid membranes, the middle NAC region with an intermediate affinity and the C-

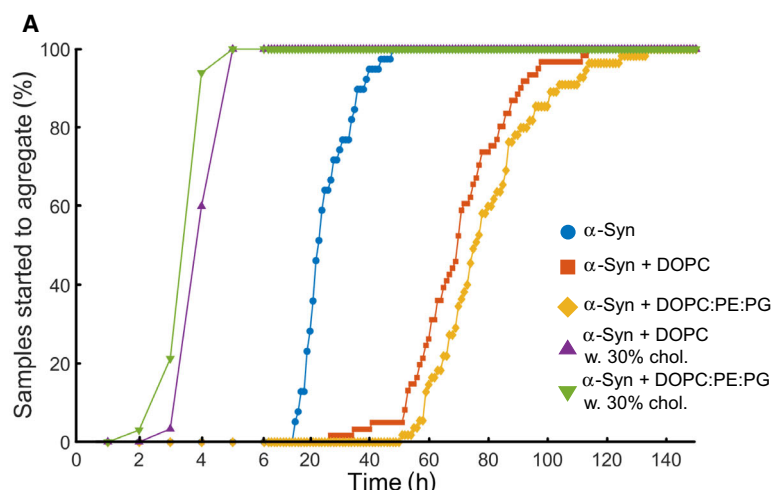
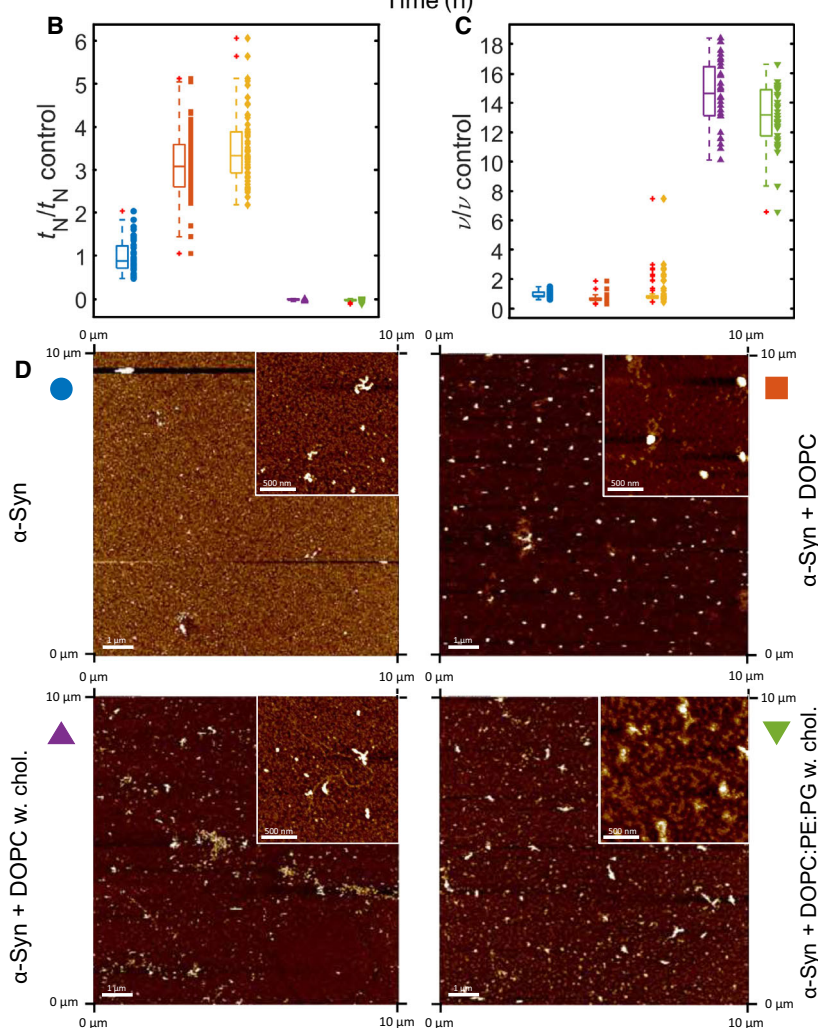


**Fig. 3.** Cholesterol promotes early oligomerization. (A) The cumulative distribution of ThT-positive wells. The number of repeats for each case is 39 ( $\alpha$ -Syn only), 30 (DOPC), 33 (DOPC : PE : PG), 61 (DOPC with cholesterol) and 55 (DOPC : PE : PG with cholesterol). Each set of repeats is generated from 3 independent experiments. (B) Ratio of  $t_N/t_{N\text{ control}}$ , which represents lag time ratio (relative primary nucleation rate). (C) Ratio of  $\nu/\nu_{\text{control}}$ , which represents the relative growth rate. (B, C) Central mark of the box indicates median; the top and bottom of the box indicate 25th and 75th percentiles, respectively. The whiskers extend to extreme data points; outliers are indicated by red '+' symbol. (D) Representative AFM images of  $\alpha$ -Syn in the presence and absence of nanodiscs with and without cholesterol. The lipid composition of the nanodiscs used in each case is indicated next to the figure panels. The images are all acquired at  $256 \times 256$  px resolution during the lag phases of the ThT-monitored fibrillation kinetics. Every sample was prepared 3 times, and for each preparation, 5 random areas were selected for imaging. Each panel shows randomly selected image of  $10 \mu\text{m} \times 10 \mu\text{m}$  size, while the insets are of  $2 \times 2 \mu\text{m}$  size. Vertical scales span from darkest to brightest colour:  $\alpha$ -Syn (2.6 nm, inset 4.0 nm),  $\alpha$ -Syn + DOPC (16.5 nm, inset 19.8 nm),  $\alpha$ -Syn DOPC with cholesterol (6.6 nm, inset 3.4 nm) and  $\alpha$ -Syn + DOPC : PE : PG with cholesterol (7.5 nm, inset 8.8 nm).



terminal with low affinity. This division is expected, as it fits well with a standard description of  $\alpha$ -Syn structure [4,62,63]. Consistent with recent research [58,64], most of the observable peaks in the C-terminal region

did not change in any way, suggesting most of the C-terminal domain remains unperturbed in a random coil formation. These peaks are depicted in Fig. 4C as deep red.

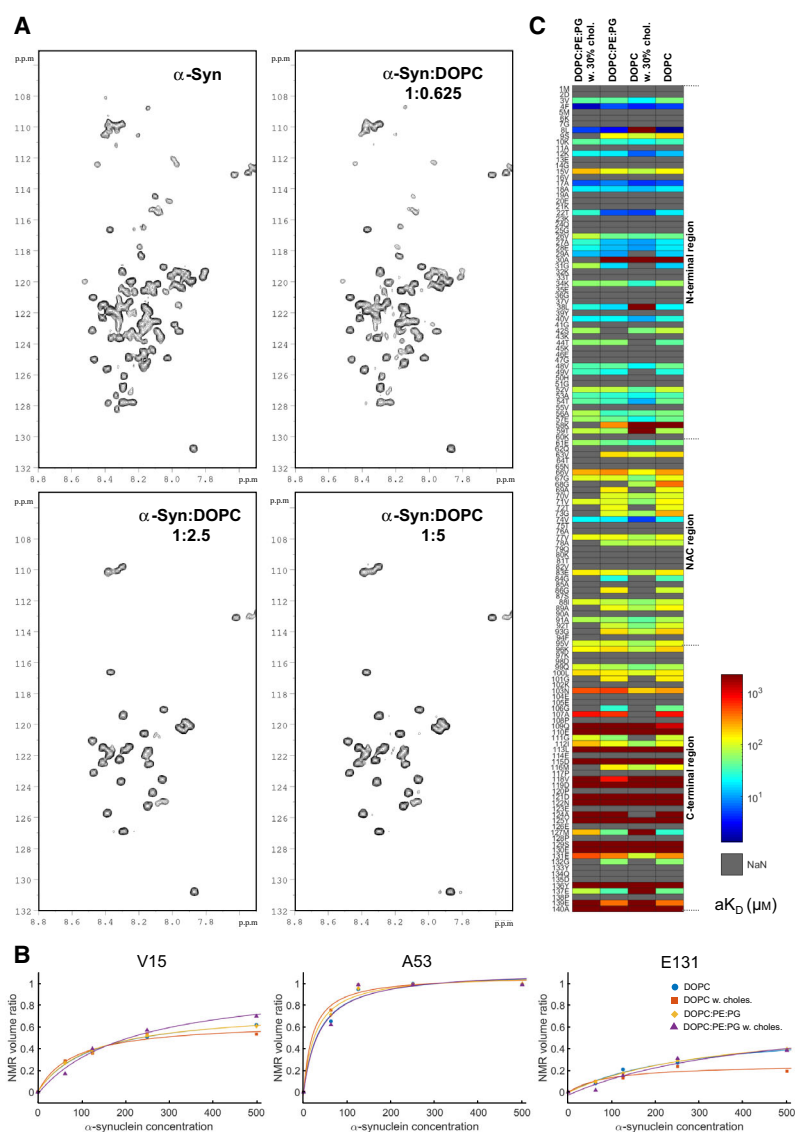
Since the presence of cholesterol has such an impact on both  $\alpha$ -Syn binding and fibrillation rates, we wanted to determine which parts of  $\alpha$ -Syn were particularly affected. Cholesterol-induced changes in the  $aK_D$  values are therefore plotted in Fig. 5A,B and projected onto the PDB model (Fig. 5C). When cholesterol is present in the lipid nanodiscs, we could see two different types of interaction behaviour. For the DOPC : PE : PG model, we observed a slight increase of  $aK_D$  in both the amphipathic and acidic region of  $\alpha$ -Syn, while the NAC region is mostly unaffected (Fig. 5B). The  $aK_D$  increase was most prominent in the C-terminal region and in several N-terminal region residues. This is in line with what was observed by SPR (Fig. 1), where cholesterol seems to inhibit the interaction of  $\alpha$ -Syn and the anionic lipid bilayer. In contrast, the trend for DOPC and cholesterol is entirely different (Fig. 5A). When cholesterol was present in DOPC lipid nanodiscs, we observed a decrease in  $aK_D$ s along almost the whole sequence of  $\alpha$ -Syn. This decrease was highest in the NAC region, which suggests that this part was the key  $\alpha$ -Syn segment in binding DOPC bilayers affected by cholesterol. However, the overall increase in  $\alpha$ -Syn  $aK_D$ s for DOPC : PE : PG nanodiscs containing cholesterol was smaller than the overall decrease in  $aK_D$ s for DOPC nanodiscs containing this lipid. This suggests that the effect of including smaller and charged head groups is higher and more pronounced than the effect of cholesterol on  $\alpha$ -Syn binding to the lipids. It should also be noted at this point that addition of cholesterol to nanodiscs also increased their diameters to almost double (Fig. 2), possibly creating more nucleation sites through size effects alone.

## Discussion

The interest in the role of lipid composition on  $\alpha$ -Syn function and dysfunction has prompted research with a variety of membrane model systems [65]. Nanodiscs comprising lipids with a variety of charges and acyl-chain saturations have been used in recent  $\alpha$ -Syn research [4,66]. In the present study for the first time, we have produced and studied the effect of cholesterol-containing nanodiscs. Inclusion of cholesterol and PE impaired disc formation, but this was overcome by adjusting the SMA concentration and by having SMA present at vesicle extrusion. SMA discs consequently proved to be versatile model systems with respect to the lipids that can be included in the bilayer. For fibrillation experiments, the nanodiscs removed reliance on unstable and insoluble vesicles, allowing much longer experiments.

The presence of lipids with a net negative charge has been established as a primary determinant for reversible protein–membrane interactions in general [67–70] and also for  $\alpha$ -Syn [4,7,36]. Other membrane-related factors reported in the literature are fluidity [4,9] and packing defects [38]. Our study shows that higher net charge and smaller head groups (from pure DOPC to a mixture of DOPC : PE : PG (4 : 3 : 1)) lead to a substantial increase in affinity (Fig. 1), consistent with earlier studies [36–39,71]. The nanodiscs have a more negative zeta potential than the corresponding vesicle except in the DOPC instance (Fig. 2), suggestive of increased binding due to this factor. The presence of cholesterol does not affect zeta potentials much, again except for the DOPC vesicle case. In fact, the substantial change (–18.7 mV for DOPC only to –6.9 mV when cholesterol is present) in zeta potential could account for much of the reduction in binding in this particular case, in accordance with results in Fig. 1E. While it has been reported that cholesterol can promote the interaction between  $\alpha$ -Syn oligomers and zwitterionic PC and PE lipids prepared as vesicles and sonicated lipid dispersions [72,73], we do not observe this for our PE-containing system. This may be due to the fact that our initial binding studies are performed with monomeric  $\alpha$ -Syn and that our model systems are different, that is, not prepared with high curvature and sonication. Aside from effects on particle zeta potential, cholesterol is well known to affect an ordering of fluid bilayers [12,74,75], a property highlighted by recent research as relevant for  $\alpha$ -Syn oligomerization behaviour [4,73]. In our study, the SPR binding experiments revealed relatively low affinity between monomeric  $\alpha$ -Syn and DOPC vesicles, while DOPC : PE : PG vesicles elicited strong binding (steady-state  $K_{DS}$  of 1.079 and 0.168  $\mu$ M, respectively). Corresponding bilayers containing cholesterol caused an almost twofold increase of  $K_D$  in both lipid models. However, the  $K_D$  for DOPC : PE : PG with 30% cholesterol was still almost four times lower than that for the DOPC membrane model. The laurdan fluorescence experiments confirmed an ordering of the bilayer when cholesterol was included (Fig. 2C–F). The experiments also suggested that the bilayers encased in nanodiscs had a more solvent-accessible lipid packing than their vesicle counterparts. The tighter and more ordered packing of lipids induced by cholesterol had a negative impact on the  $\alpha$ -Syn bilayer interaction, although even with a cholesterol content of 30%, all of our vesicle membrane model systems are expected to be fluid and miscible at 310 K [74–76]. While the changes in observed binding cannot then be directly attributed to the presence of ordered phases, our





findings are consistent with recent reports, finding that bilayer fluidity is an essential driver for binding alongside charge [4,72].

Nanodiscs allowed us to investigate the protein conformational response by NMR, but the problem with protein states that are invisible to NMR remains due to a combination of complex chemical exchange between protein states and line-broadening effects due to efficient relaxation [4,77]. The nanodiscs in combination with the stochastic approach adapted from Afitska *et al.* [52], made it possible to investigate the effect of membrane components on fibrillation rates while avoiding experimental sensitivity to initial conditions, that otherwise would be difficult to control for. The onset of  $\alpha$ -Syn fibrillation was delayed in the

presence of lipid nanodiscs lacking cholesterol (Fig. 3). In the presence of both DOPC and DOPC : PE : PG nanodiscs, there was almost a threefold increase in  $\alpha$ -Syn fibrillation lag time (Fig. 3B). This observation is similar to other reports where  $\alpha$ -Syn fibrillation is delayed by the presence of lipids [36,37,52]. Moreover, no significant changes in the fibrillation rate were observed (Fig. 3C). This suggests that the lipids effectively decrease the population of free  $\alpha$ -Syn monomers, leaving less protein available for oligomerization and fibrillation. Surprisingly, this is also observed in the presence of zwitterionic DOPC to which  $\alpha$ -Syn has a very low affinity. It seems that even this low affinity is sufficient to almost double lag times for the onset of fibrillation. These observations are consistent with the

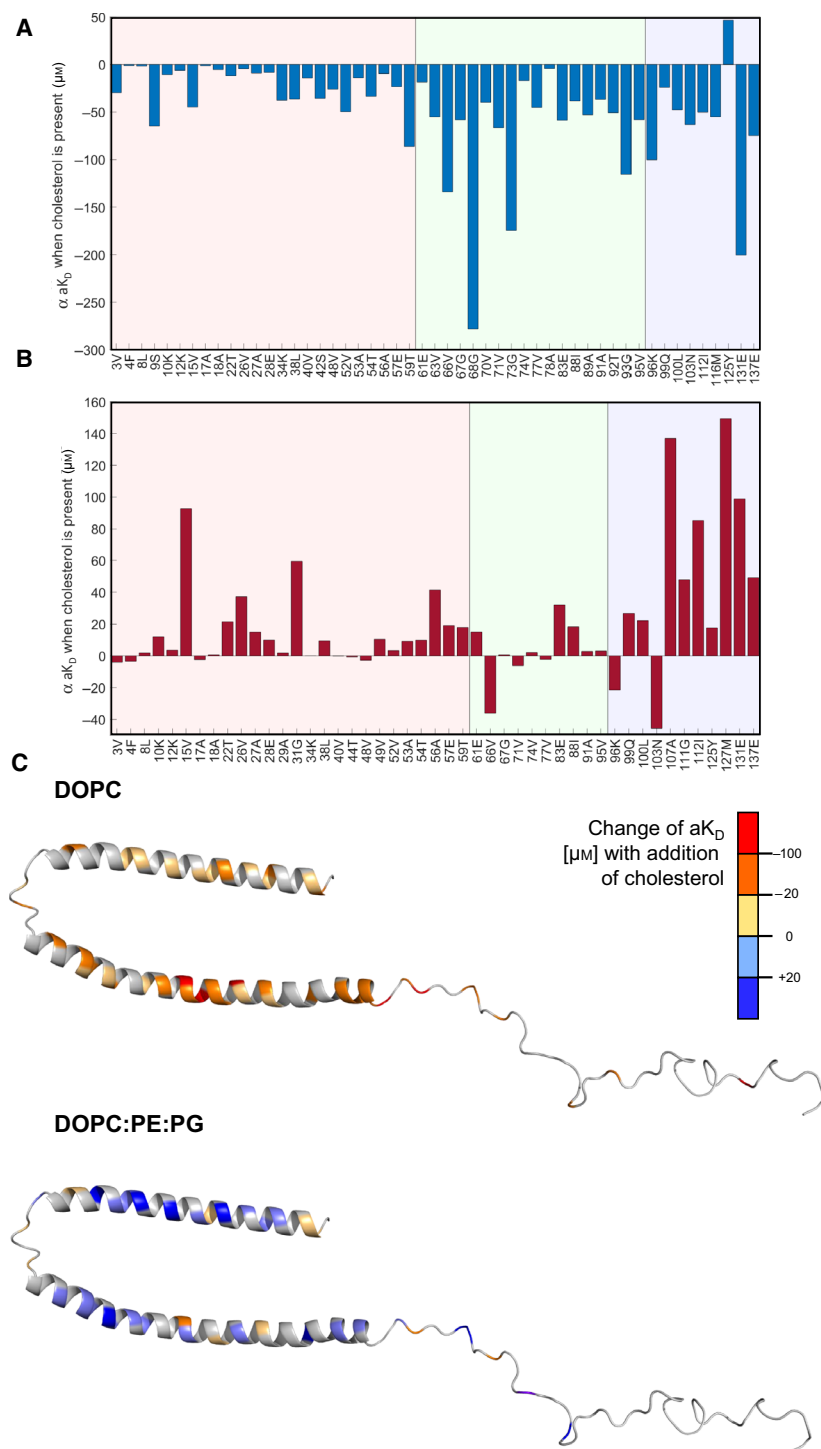


**Fig. 5.** Cholesterol in noncharged nanodiscs promotes site-specific  $\alpha$ -Syn binding. (A, B) Bar plot of  $aK_D$  difference for samples with and without cholesterol for DOPC (A) and DOPC : PE : PG (B) lipid nanodiscs. Only amino acids with  $r^2 > 0.90$  for both samples are shown. The sequence is visually divided into three parts of the  $\alpha$ -Syn protein: the N-terminal amphipathic region, the NAC region and the C-terminal acidic tail (light red, light green and light blue, from left to right). (C) Representation of the estimated difference of  $aK_D$  values after the addition of cholesterol. The representation was prepared in PyMOL (Schrödinger, Inc.), using PDB entry 1XQ8 as a template.

AFM images of DOPC nanodisc, where discs appear to keep  $\alpha$ -Syn aggregates from appearing on the background (Fig. 3D). The potential for using zwitterionic small unilamellar vesicles to inhibit the onset of  $\alpha$ -Syn fibrillation and protect dopaminergic cells has recently

been reported by Aliakbari *et al.* [66] It seems that  $\alpha$ -Syn engages in a dynamic exchange with PC and PE membrane components that do not give rise to high-affinity binding, but is nonetheless very important for preventing nucleation with subsequent fibrillation.

The presence of cholesterol in the lipid nanodiscs caused a significant promotion of  $\alpha$ -Syn fibrillation (Fig. 3). The lag times decreased almost to zero (Fig. 3 B) and fibrillation rate increased to more than 13 times that of  $\alpha$ -Syn alone (Fig. 3C). One possible explanation for these dramatic changes is that lipid nanodiscs containing cholesterol served as a seeding agent, independently of other lipids present. Other reports on the effect of cholesterol on  $\alpha$ -Syn fibrillation are conflicting, possibly because factors such as curvature, phase behaviour or miscibility of the lipid mixes in use are not comparable. Simple size effects may also play a role. Addition of cholesterol doubles the average nanodisc sizes (Fig. 2). Some studies using lipid vesicles did not observe any promotion of  $\alpha$ -Syn fibrillation by lipid vesicles containing cholesterol [28,66], while other studies observed increased oligomerization in the presence of oxidized cholesterol metabolites [78] or increased fibrillation and deposit formation in cell cultures exposed to higher cholesterol concentrations [79]. The lipid nanodiscs used in our experiments are much smaller (see Fig. 2A) than vesicles used in previous experiments, and there is no bilayer curvature. Our results are supportive of a planar bilayer being able to promote, when cholesterol is present, colocalization and co-orientation of  $\alpha$ -Syn molecules in a spatially restricted area. This effect of local enrichment of  $\alpha$ -Syn on membranes and molecular crowding has been suggested as the mechanism of  $\alpha$ -Syn fibrillation in live cells [80]. However, it is still unclear whether cholesterol plays a unique role in this, as evidence exists for ordered, planar bilayers promoting  $\alpha$ -Syn fibrillation in the absence of cholesterol [4].

Using the approach of Shortridge *et al.* [34] it was possible to determine  $aK_D$  values for individual residues in the  $\alpha$ -Syn primary sequence and in this way gain some insight into how different membrane components affect different parts of the protein. The  $aK_D$  values do not differentiate between the possible causes of line broadening, but reflects the net effect the nanodiscs have on diminishing the protein signals. While the approach yielded valuable information, we could observe and fit only 48% of the amino acid sequence. This number is reduced for samples containing 30% cholesterol. The undetectable amino acid states suggest that protein–lipid, protein–protein or intramolecular exchange takes place on a timescale unfavourable for NMR observation. Most of the lysines, which have a strong electrostatic affinity for lipid head groups [37,71], were not observed in the presence of lipids. In fact, if we inspect amino acids which correspond to undetectable peaks and where they appear in the sequence (Fig. 4C), we find that most invisible states

are organized in nonperfect hexameric KTKEGV repeats, which represent a small  $\alpha$ -helical motif with high affinity to lipid environment [37,62,81,82]. The fact that the presence of cholesterol causes more  $\alpha$ -Syn residues in these repeats to become undetectable suggests that these are affected by the presence of cholesterol. This is particularly apparent in the N-terminal region and NAC region, where we observed a longer stretch of invisible peaks in the T72–V82 region. This stretch coincides with the ending of the NAC core, which has been proposed to function as a sensor of the state of the lipid bilayer [56] and which participates in the formation of  $\beta$ -sheets during oligomerization [83]. Notably, this invisible stretch is extended when the cholesterol is present, particularly in the presence of DOPC : PE : PG with 30% cholesterol nanodiscs, indicating that the NAC region is affected by the ordering effect that cholesterol has upon the bilayer. We also observed several disappearing peaks in the C-terminal (especially in the interval G132–D135) which is, generally, regarded as nonreactive towards lipids but protective against aggregation [84,85]. This suggests a chaperone-like activity for this region, maintaining at least some protein interaction with the solvent rather than allowing it to nucleate at the membrane or other potential seeding sites, as has been suggested by other authors [52,85]. The influence of cholesterol on this part of the protein would interfere with the moderating effect of the C-terminal, contributing to accelerated nucleation of  $\alpha$ -Syn. Interestingly, it has recently been shown that the C-terminal helps to modulate  $\alpha$ -Syn membrane interaction and its localization at the presynaptic terminal by binding to  $\text{Ca}^{2+}$  [64]. Moreover, natively occurring C-terminally truncated  $\alpha$ -Syn is associated with increased fibrillation, a phenomenon that was further enhanced, if known disease mutants were present in the fibrillation assays [85].

In our study, we have shown that the presence of cholesterol has an overall inhibitory effect on  $\alpha$ -Syn to lipid vesicles. However, we have also observed that lipid nanodiscs containing cholesterol can act as a strong promoter of  $\alpha$ -Syn fibrillation. Both inhibition of  $\alpha$ -Syn binding to vesicles and promotion of  $\alpha$ -Syn fibrillation by lipid nanodiscs are seemingly independent of lipid composition as they are similar for both DOPC and DOPC : PE : PG (4 : 3 : 1) lipid models. Still, when investigated by NMR we find that the effect of cholesterol on  $\alpha$ -Syn is fundamentally different for different lipid bilayers. In zwitterionic lipid models (DOPC), it is the NAC region which is affected the most by the presence of cholesterol, while in the DOPC : PE : PG lipid model, it is the C-terminal and

several N-terminal residues. The recently published model of Viennet *et al.* [4] for  $\alpha$ -Syn-lipid interaction and fibrillation was able to rationalize fibrillation in terms of lipid charge and fluidity; in this model, a paucity of high-affinity charged sites may lead to molecular crowding, where NAC segments are aligned at sites in the liquid-ordered phase, resulting in accelerated oligomerization. Relating our results to this model, we propose that cholesterol-rich regions could act as such nucleation sites. If sites with a net negative charge are not available, cholesterol-rich sites will become the next preferred site for binding and potential crowding. Cholesterol, through its ordering effects on the membrane, would make it harder for a polypeptide to intercalate into the bilayer [12,86,87], leaving more scope for protein-protein interaction at the water-lipid interface. This difference in  $\alpha$ -Syn binding behaviour could be used to explain some discrepancy between observed  $\alpha$ -Syn interactions with cholesterol, primarily by making a distinction between a cholesterol-rich, NAC-supported binding mode and a high-charge, high-fluidity mode supported primarily by the N-terminal. Both modes can lead to increased fibrillation if molecular crowding occurs at the available sites, but cholesterol strongly promotes these events independently of net charge. Given the high amount of cholesterol in the synaptic membrane, this suggests that  $\alpha$ -Syn must neither overload potential nucleation sites nor remain at such sites for an extended time. A possible interaction partner of  $\alpha$ -Syn that might alleviate such overload is the ubiquitous 14-3-3 proteins that normally have roles as scaffolding proteins that bring other proteins together. Several of the isoforms (seven in humans) of this protein class have been identified in Lewy bodies [88,89]. Interaction studies of the  $\eta$ -isoform and  $\alpha$ -Syn showed that it binds to oligomeric but not monomeric  $\alpha$ -Syn, and intriguingly, this isoform is also present in the synaptic membrane and synaptic junctions [90]. In addition, the isoform was shown to reduce  $\alpha$ -Syn toxicity in cell models [91]. These observations suggest that 14-3-3 proteins may be involved in handling  $\alpha$ -Syn overload situations at cholesterol-rich sites and may provide a link between the lipid membrane and the proteostasis network.

## Materials and methods

### Recombinant $\alpha$ -Syn expression and purification

For use in this study, we modified the vector pET21a- $\alpha$ -synuclein (Addgene plasmid 51486) by introducing a 6x-histidine tag followed by a TEV cleavage site to the N-terminal of  $\alpha$ -Syn. This was achieved with the Q5<sup>®</sup>

Site-Directed Mutagenesis Kit (New England Biolabs, Hitchkin, UK) using the primers listed in the Supplementary information (Table S3).

Unlabelled  $\alpha$ -Syn was expressed and purified using a variant of a previously described protocol [92]. The plasmid encoding  $\alpha$ -Syn was transformed into *E. coli* BL21 Star<sup>™</sup> (DE3) (Invitrogen, Waltham, UK) following manufacturer's instructions and plated onto lysogeny broth (LB) agar plates supplemented with 100  $\mu\text{g}\cdot\text{mL}^{-1}$  ampicillin. Single colonies were used to inoculate 10 mL overnight starter cultures. The following day, the overnight culture was used to inoculate 1-litre cultures. All the cultures were grown in media supplemented with 100  $\mu\text{g}\cdot\text{mL}^{-1}$  ampicillin using orbital shakers at 37 °C and 250 r.p.m. Protein expression was induced when the cultures reached an optical density of 0.4 (OD<sub>620</sub>) by the addition of IPTG to a final concentration of 0.1 mM. Cells were harvested after 5 h by centrifugation (10 000 *g* for 20 min). The obtained bacterial pellets were resuspended in 20 mL osmotic shock buffer (30 mM Tris/HCl [pH 8.0], 40% saccharose and 2 mM EDTA) per gram cell wet weight before 10-min incubation at room temperature. Following the osmotic shock, the cells were collected by centrifugation (20 000 *g* for 20 min) and the content of the periplasmic space was released by adding 45 mL ice-cold water containing 1 mM MgCl<sub>2</sub>. Cell debris was removed with centrifugation (20 000 *g* for 20 min). The supernatant containing  $\alpha$ -Syn was mixed with Na<sub>2</sub>HPO<sub>4</sub> to a final concentration of 20 mM Na<sub>2</sub>HPO<sub>4</sub> [pH 7.4] and supplemented with cComplete<sup>™</sup> EDTA-free protease inhibitors (Roche, Basel, Switzerland).

$\alpha$ -Syn was further purified with Ni-NTA affinity chromatography using a HisTrap HP 5-mL column (GE Healthcare Life Sciences, USA) connected to an ÄKTA system (GE Healthcare Life Sciences). The Ni-NTA purification was performed using buffer A (20 mM Tris, 150 mM NaCl and 20 mM imidazole [pH 8.0]) and buffer B (20 mM Tris, 150 mM NaCl and 500 mM Imidazole [pH 8]). After elution, the buffer was changed into TEV cleavage buffer (20 mM Tris, 0.5 mM EDTA, 1 mM DTT and 150 mM NaCl [pH 8.0]) using PD-10 columns (GE Healthcare Life Sciences, Chicago, IL, USA).

The concentration of uncleaved  $\alpha$ -Syn was determined using an extinction coefficient at 280 nm of 7450  $\text{M}^{-1}\cdot\text{cm}^{-1}$ . TEV (produced in-house according to van den Berg *et al.* [93]) was added to  $\alpha$ -Syn in a 1 : 100 molar ratio (TEV :  $\alpha$ -Syn) and incubated for 16 h at 4 °C. After the cleavage,  $\alpha$ -Syn was collected by elution in another Ni-NTA affinity chromatography step. Lastly,  $\alpha$ -Syn was purified by size-exclusion chromatography using a HiLoad Superdex column 16/600 75  $\mu\text{g}$  (GE Healthcare Life Sciences) connected to an ÄKTA system (GE Healthcare Life Sciences). The concentration of purified  $\alpha$ -Syn was determined using an extinction coefficient at 280 nm of 5960  $\text{M}^{-1}\cdot\text{cm}^{-1}$ . Typical yield was 15 mg of cleaved protein per litre of medium.



For isotopic labelling, we adapted a previously published technique in which the culture is initially grown using LB [94,95]. The culture was grown identically to the unlabelled up to the point where the optical density reached 0.7. At this point, the cells were harvested and resuspended into M9 salt wash medium (25 mM  $\text{KH}_2\text{PO}_4$ , 10 mM NaCl, 5 mM  $\text{MgSO}_4$  and 0.2 mM  $\text{CaCl}_2$  [pH 8.0]). Following a subsequent centrifugation (10 000 *g* for 20 min) step, the cells were resuspended in modified Marley minimal medium (25 mM  $\text{KH}_2\text{PO}_4$  [pH 8.0], 10 mM NaCl, 5 mM  $\text{MgSO}_4$ , 0.2 mM  $\text{CaCl}_2$ , 1 $\times$  trace metal solution according to Studier [95], 0.25 $\times$  vitamins (100 $\times$  BME vitamin stock solution, Sigma-Aldrich, Saint-Louis, MO, USA), 0.1%  $^{15}\text{NH}_4\text{Cl}$  and 1.0% glucose or  $^{13}\text{C}$ -glucose). The medium was added in a 1 : 4 (v/v) ratio, that is, 250 mL of 4M media was added for each 1 L of initial LB culture. The cultures were further grown for 1 h at 37 °C. Expression was induced by adding IPTG to a final concentration of 0.8 mM, and the cells were grown for 5 h in orbital shakers at 37 °C and 250 r.p.m. Further purification was identical to the unlabelled protein purification.

### Preparation of Large unilamellar vesicles

LUVs were prepared using standard methods [96]. In brief, lipid/cholesterol mixtures were prepared by dissolving defined amounts of dried lipid powders (DOPC, DOPE, DOPG and cholesterol from Avanti, USA) in 3 : 1 dichloromethane : methanol mixtures followed by drying using nitrogen gas and lastly in vacuo. The lipid films were hydrated to 20 mM concentration of lipids by adding 50 mM Tris/HCl [pH 8.0]. The hydrated lipids were subsequently subjected to 4 rapid freeze-thaw cycles ( $-195$  °C to  $+60$  °C) and extruded (13 passes) through a 100-nm polycarbonate filter (Mini-Extruder; Avanti Polar Lipids, Alabaster, Alabama, USA). The sizes of vesicles were measured by dynamic laser light-scattering system (DLS) using Zetasizer Nano ZS (Malvern Instruments, Malvern, UK). The mean size of all vesicles was  $100 \pm 6$  nm with a polydispersity index  $< 0.1$ .

### Nanodisc preparation and characterization

SMA was prepared as described previously [97]. Briefly, XIRAN SZ30010 (Polyscope, Geleen, the Netherlands) was refluxed for 4 h in 5 % (w/v) in 1 M KOH. Once cool, 6 M HCl was added dropwise to the solution at room temperature to a final concentration of 1.1 M, yielding a precipitate. The precipitate was washed 3 times with 50 mL of 100 mM HCl and then with 50 mL water. The precipitate was then freeze-dried. The loss of the anhydride groups was demonstrated by FTIR spectroscopy through the appearance of a maleic acid carbonyl stretch at  $1570\text{ cm}^{-1}$  and the loss of the maleic anhydride carboxyl stretch at  $1780\text{ cm}^{-1}$ . The polymer was stored as a solution of 8% (w/v) SMA in

50 mM Tris/HCl (pH 8.0) at  $-80$  °C and was used without further purification.

Nanodiscs were prepared using a modified procedure based on Scheidelaar *et al.* [98] Hydrated lipids and SMA were mixed in varying ratio based on nanodisc composition (see Table S1). The mixture was processed in the same manner as hydrated lipids in LUV preparation (4 freeze-thawing cycles and 13 extrusion cycles through a 100-nm filter), and incubated overnight at room temperature. Nanodiscs were further purified by size-exclusion chromatography using HiLoad Superdex column 16/600 200 pg (GE Healthcare Life Sciences) connected to an ÄKTA system. The fractions containing the desired nanodiscs were collected, and their size and zeta potential were determined by DLS using (Nanosizer ZS Malvern Instruments). The mean values of major nanodiscs peaks are shown in Fig. 1A.

The lipid concentrations of the nanodiscs was determined by taking 100  $\mu\text{L}$  of the purified nanodiscs, freeze-drying them overnight (Alpha 1-2 LDplus, Christ, Osterode am Harz, Germany), dissolving them in 300  $\mu\text{L}$  of CUBO solvent (800  $\mu\text{M}$  guanidine chloride in mixture of dimethylformamide (DMF) and trimethylamine (3 : 1); 20 % of DMF was d-7 deuterated; Sigma-Aldrich) containing 50  $\mu\text{M}$  trimethyl phosphate standard (Sigma-Aldrich) and collecting  $^{31}\text{P}$  NMR with AVANCE™ III HD 600 MHz NMR instrument (Bruker Biospin AG, Fällanden, Switzerland).

Fluidity and packing of nanodiscs were explored by 6-dodecanoyl-N,N-dimethyl-2-naphthylamine (Laurdan, Sigma-Aldrich). Nanodiscs/vesicles (100  $\mu\text{M}$ ) and laurdan (1  $\mu\text{M}$ ) were incubated at 37 °C, and fluorescence excitation and emission were measured by PerkinElmer Fluorescence Reader LS-55 (PerkinElmer, Waltham, MA, USA). Excitation and emission spectra were measured with fixed wavelength—430 and 390 nm, respectively. Generalized polarizations plots were calculated for temperatures 10, 20, 30 and 31 °C (Fig. S2).

### SPR assays

The SPR experiments were conducted in room temperature using a T200 Biacore instrument (GE Healthcare) on an L1 chip. The surface of the L1 chip was conditioned with three consecutive 1-minute injections of 20 mM CHAPS followed by one injection of 30% ethanol. The flow rate for these injections was  $30\ \mu\text{L}\cdot\text{min}^{-1}$ . Liposomes (10 mM in PBS) were deposit in all cells for 40 min at a flow rate of  $2\ \mu\text{L}\cdot\text{min}^{-1}$ . The surface was stabilized by three injections containing 100 mM NaOH for 1 min using a flow rate of  $30\ \mu\text{L}\cdot\text{min}^{-1}$ . The successful surface coverage was tested by injecting  $0.1\ \text{mg}\cdot\text{mL}^{-1}$  of bovine serum albumin (BSA) for 1 min at  $30\ \mu\text{L}\cdot\text{min}^{-1}$ , and a change of  $< 400$  RU indicated sufficient coverage. Between experiments, the chip surface was cleaned by subsequent injection of 20 mM CHAPS,

40 mM octyl  $\beta$ -D-glucopyranoside and 30% ethanol, each for 1 min at  $30 \mu\text{L}\cdot\text{min}^{-1}$ .

For all measurement, the flow rate was fixed at  $15 \mu\text{L}\cdot\text{min}^{-1}$ . Dilutions of  $\alpha$ -Syn (from  $8 \mu\text{M}$  to  $0.063 \mu\text{M}$ , in 20 mM sodium phosphate [pH 6], 100 mM NaCl) were injected over immobilized liposomes on the L1 chip. Injections were made from low to high concentration with 250-s contact time and 400-s dissociation phase. Liposomes were then regenerated by three subsequent injections of 100 mM NaOH at  $30 \mu\text{L}\cdot\text{min}^{-1}$  for 1 min. The RU stability was checked, and experiments were only executed if the RU was in the range of  $\pm 200$  prior to the  $\alpha$ -Syn injection. The control flow cell was treated the same way as sample cells (liposome coverage, stabilization, BSA coverage, regeneration and cleaning) except that  $\alpha$ -Syn injections were replaced with buffer (20 mM sodium phosphate [pH 6] and 100 mM NaCl). Control flow cell background was subtracted from the experimental cell before further data processing. The data points for steady-state affinity analysis were taken after 240-sec injection. The resulting curves were fitted into Eqn (1) using in-laboratory written MATLAB script (MATLAB R2017b).

$$R_{\text{eg}} = \frac{c \cdot R_{\text{max}}}{K_{\text{D}} + c} + R_{\text{off}}. \quad (1)$$

Steady-state SPR interaction fitting model where  $R_{\text{eg}}$  = response at equilibrium,  $c$  = concentration of  $\alpha$ -Syn,  $R_{\text{max}}$  = maximum response,  $K_{\text{D}}$  = dissociation constant and  $R_{\text{off}}$  = response offset.

### ThT and TPE-TPP assay

The aggregation experiments of  $\alpha$ -Syn were performed at  $37^\circ\text{C}$  using a FLUOstar Optima microplate fluorescence reader (BMG LABTECH, Mölndal, Sweden) and monitored by thioflavin T (ThT, Sigma-Aldrich) and TPE-TPP (a kind gift from Ben Zhong Tang [35]) fluorescence. The fluorescence was measured at time intervals of 600 s with for 150 h. Before each measurement 3 mm orbital shaking for 300 s was applied. The excitation and emission wavelengths were 430 (10) nm and 485 (5) nm for ThT and 360 (10) nm and 420 (10) nm for TPE-TPP. Lamp settings were as follows: 10 flashes per well and 1300 gain for ThT and 1900 gain for TPE-TPP. Experiments were performed using black 384-well plate with clear bottom (Corning, New York, NY, USA, Cat. N. 3762) sealed with sealing tape (Thermo Fisher Scientific, Waltham, MA, USA, Cat. N. 232701) to prevent evaporation. The aggregation buffer contained 20 mM sodium phosphate [pH 6], 100 mM NaCl, 10 mM  $\text{NaN}_3$  and 1 mM EDTA. The final concentrations of the components in the wells were  $60 \mu\text{M}$   $\alpha$ -Syn,  $5 \mu\text{M}$  ThT or TPE-TPP, and none or 1 mM of the lipid nanodiscs. Buffer and lipids alone were also measured as controls. We performed three

independent experiments with 8–12 repeats for each sample. The recorded curves were processed using in-laboratory written MATLAB script (MATLAB R2017b). Similar to the work of Aftiska *et al.* [52], cumulative curves were recorded evaluating the percentage of wells having a signal three times higher than noise (mean of control wells containing all the components except  $\alpha$ -Syn). Each curve was also fitted with Finke–Watzky two-step model Eqns (2) and (3), and  $t_{\text{n}}$  and  $\nu$  were calculated [53].

$$F(t) = \frac{1}{1 + e^{-4\nu(t-t_{1/2})}}. \quad (2)$$

$$t_{\text{n}} = t_{1/2} - \frac{1}{2\nu}. \quad (3)$$

The Finke–Watzky two-step model [53], where  $t_{1/2}$  is a half time of fibrillation,  $\nu$  is growth rate, and  $t_{\text{n}}$  is lag time.

### Atomic force microscopy

Samples for AFM analysis were prepared in the following way.  $2 \mu\text{L}$  of sample solution was deposited on a freshly cleaved mica disc and left for 30 min in a closed Petri dish (plastic, 50 mm in diameter). After deposition,  $100 \mu\text{L}$  of Milli-Q water (filtered and de-ionized  $18.2 \text{ M}\Omega\cdot\text{cm}$  at  $25^\circ\text{C}$ ) was added to each mica disc and incubated for one minute with subsequent excess water removal by using paper tissues. This procedure was applied three times, and samples were left to dry in a closed Petri dish for two hours. Sample morphologies were studied using a Bruker Bioscope Catalyst Microscope in a Peak Force Quantitative Nanomechanical Property Mapping mode. Silicon Nitride Bruker ScanAsyst Air cantilevers with  $\sim 2\text{-nm}$  tip radius and  $\sim 25^\circ$  tip angle were used for imaging. Images were taken at  $256 \times 256$  px resolution. At least five images were taken for each sample, which were at least  $50 \mu\text{m}$  apart from each other to ensure that the morphologies shown are representative.

### NMR spectroscopy

$2\text{D } ^1\text{H-}^{15}\text{N}$  HSQC NMR spectra of  $0.1 \text{ mM}$  uniformly labelled  $^{15}\text{N}$   $\alpha$ -Syn in 20 mM sodium phosphate [pH 6], 100 mM NaCl and 10%  $\text{D}_2\text{O}$  were measured at 299 K using 850 MHz (Bruker). We used best-HSQC (b\_hsqcetf3gpsi)<sup>94</sup> and DOSY (stebpgls19) standard pulse programmes supplied in TopSpin 4.0.1. Spectra were recorded in the absence or presence of lipid nanodiscs at 500, 250, 125 or  $62.5 \mu\text{M}$  total lipid concentration. Data were processed using TopSpin, PINT [99] and in-laboratory written MATLAB scripts (MATLAB 2017b). Apparent  $K_{\text{D}}$  ( $aK_{\text{D}}$ ) calculations were done according to Shortridge *et al.* [34], and the area of deconvoluted peaks from PINT was used to calculate peak volume ratio

$B = 1 -$  (bound peak volume/free peak volume) and fitted according to Eqn (4).

$$B = 1 - \frac{V_B}{V_F} = 1 - \frac{1}{1 + \frac{c[P]_T}{[L]_T + aK_D}} + n[L]_T. \quad (4)$$

Protein–ligand binding model based on Shortridge *et al.* [34] where  $B$  is the NMR volume ratio,  $V_B$  the peak volume in bounded state,  $V_F$  the peak volume in free state,  $c$  the unitless NMR area ratio constant,  $[P]_T$  the total protein concentration,  $[L]_T$  the total lipid concentration,  $aK_D$  the apparent dissociation constant and  $n$  the nonspecific binding constant.

## Acknowledgements

This work was primarily financed through the Research Council of Norway grant NFR240063. The authors would like to thank the staff at the NNP Bergen node for facilitating the NMR experimental work, the laboratory of Professor Ben Zhong Tang for providing TPE-TPP, Stefan Scheidelaar at Polyscope, Jonas Dörr at University of Utrecht, for providing SMA, and Vinnit Georg for preparing samples. This work was also partly supported by Bergen Research Foundation, Sparebankstiftinga Sogn og Fjordane and the Research Council of Norway through the Norwegian NMR Platform, NNP (226244/F50). LAM-R acknowledges the Swedish Research Council for financial support.

## Conflict of interest

The authors declare no conflict of interest.

## Author contributions

ØH and MJ conceived the research questions. ØH, MJ and SF designed the experiments. MJ and SF established the lipid nanodiscs. ML established the  $\alpha$ -Syn expression. MJ and DT collected and analysed the SPR data. MJ, EB and ØH collected and analysed the NMR data. IAI and LAM-R performed and analysed the AFM. MJ, EB, VG and IAI carried out all other laboratory work. ØH conceived, designed and wrote the grant proposal and the research programme. All authors interpreted data and commented on the final version of the manuscript.

## References

1 Winner B, Jappelli R, Maji SK, Desplats PA, Boyer L, Aigner S, Hetzer C, Loher T, Vilar M, Campioni S *et al.* (2011) In vivo demonstration that alpha-synuclein

oligomers are toxic. *Proc Natl Acad Sci USA* **108**, 4194–4199.

- 2 Logan T, Bendor J, Toupin C, Thorn K & Edwards RH (2017)  $\alpha$ -Synuclein promotes dilation of the exocytotic fusion pore. *Nat Neurosci* **20**, 681–689.
- 3 Galvagnion C (2017) The role of Lipids Interacting with  $\alpha$ -Synuclein in the pathogenesis of Parkinson's disease. *J Parkinsons Dis* **7**, 433–450.
- 4 Viennet T, Wördehoff MM, Uluca B, Poojari C, Shaykhalishahi H, Willbold D, Strodel B, Heise H, Buell AK, Hoyer W *et al.* (2018) Structural insights from lipid-bilayer nanodiscs link  $\alpha$ -Synuclein membrane-binding modes to amyloid fibril formation. *Commun Biol* **1**, 44.
- 5 Jo E, McLaurin JA, Yip CM, St. George-Hyslop P & Fraser PE (2000)  $\alpha$ -Synuclein membrane interactions and lipid specificity. *J Biol Chem* **275**, 34328–34334.
- 6 Galvagnion C, Buell AK, Meisl G, Michaels TCT, Vendruscolo M, Knowles TPJ & Dobson CM (2015) Lipid vesicles trigger  $\alpha$ -synuclein aggregation by stimulating primary nucleation. *Nat. Chem. Biol.* **11**, 229–234.
- 7 Middleton ER & Rhoades E (2010) Effects of curvature and composition on  $\alpha$ -synuclein binding to lipid vesicles. *Biophys J* **99**, 2279–2288.
- 8 Aksnes H, Ree R & Arnesen T (2019) Co-translational, post-translational, and non-catalytic roles of N-terminal acetyltransferases. *Mol Cell* **73**, 1097–1114.
- 9 O'Leary EI, Jiang Z, Strub MP & Lee JC (2018) Effects of phosphatidylcholine membrane fluidity on the conformation and aggregation of N-terminally acetylated  $\alpha$ -Synuclein. *J Biol Chem* **293**, 11195–11205.
- 10 Maltsev AS, Ying J & Bax A (2012) Impact of N-terminal acetylation of  $\alpha$ -synuclein on its random coil and lipid binding properties. *Biochemistry* **51**, 5004–5013.
- 11 van Meer G & de Kroon AIPM (2011) Lipid map of the mammalian cell. *J Cell Sci* **124**, 5–8.
- 12 Róg T, Pasenkiewicz-Gierula M, Vattulainen I & Karttunen M (2009) Ordering effects of cholesterol and its analogues. *Biochim Biophys Acta Biomembr* **1788**, 97–121.
- 13 Robinson AJ, Richards WG, Thomas PJ & Hann MM (1995) Behavior of cholesterol and its effect on head group and chain conformations in lipid bilayers: a molecular dynamics study. *Biophys J* **68**, 164–170.
- 14 Kojro E, Gimpl G, Lammich S, Marz W & Fahrenholz F (2001) Low cholesterol stimulates the nonamyloidogenic pathway by its effect on the alpha-secretase ADAM 10. *Proc Natl Acad Sci* **98**, 5815–5820.
- 15 Simons M, Keller P, De Strooper B, Beyreuther K, Dotti CG & Simons K (1998) Cholesterol depletion inhibits the generation of beta-amyloid in hippocampal neurons. *Proc Natl Acad Sci USA* **95**, 6460–6464.

- 16 Valenza M, Rigamonti D, Goffredo D, Zuccato C, Fenu S, Jamot L, Strand A, Tarditi A, Woodman B, Racchi M *et al.* (2005) Dysfunction of the cholesterol biosynthetic pathway in Huntington's disease. *J Neurosci* **25**, 9932–9939.
- 17 Vance JE (2010) Transfer of cholesterol by the NPC team. *Cell Metab* **12**, 105–106.
- 18 Wang ML, Motamed M, Infante RE, Abi-Mosleh L, Kwon HJ, Brown MS & Goldstein JL (2010) Identification of surface residues on Niemann-Pick C2 essential for hydrophobic handoff of cholesterol to NPC1 in lysosomes. *Cell Metab* **12**, 166–173.
- 19 Wood WG, Igbavboa U, Müller WE & Eckert GP (2011) Cholesterol asymmetry in synaptic plasma membranes. *J Neurochem* **116**, 684–689.
- 20 Arenas F, Garcia-Ruiz C & Fernandez-Checa JC (2017) Intracellular cholesterol trafficking and impact in neurodegeneration. *Front Mol Neurosci* **10**, 1–25.
- 21 Egawa J, Pearn ML, Lemkuil BP, Patel PM & Head BP (2016) Membrane lipid rafts and neurobiology: age-related changes in membrane lipids and loss of neuronal function. *J Physiol* **594**, 4565–4579.
- 22 Hu G, Antikainen R, Jousilahti P, Kivipelto M & Tuomilehto J (2008) Total cholesterol and the risk of Parkinson disease. *Neurology* **70**, 1972–1979.
- 23 Powers KM, Smith-Weller T, Franklin GM, Longstreth WT, Swanson PD, Checkoway H & Checkoway H (2009) Dietary fats, cholesterol and iron as risk factors for Parkinson's disease. *Parkinsonism Relat Disord* **15**, 47–52.
- 24 Huang X, Auinger P, Eberly S, Oakes D, Schwarzschild M, Ascherio A, Mailman R & Chen H (2011) Serum cholesterol and the progression of Parkinson's disease: results from DATATOP. *PLoS One* **6**, e22854.
- 25 Di Scala C, Yahi N, Boutemour S, Flores A, Rodriguez L, Chahinian H & Fantini J (2016) Common molecular mechanism of amyloid pore formation by Alzheimer's  $\beta$ -amyloid peptide and  $\alpha$ -synuclein. *Sci Rep* **6**, 1–10.
- 26 Fantini J, Di Scala C, Yahi N, Troadec JD, Sadelli K, Chahinian H & Garmy N (2014) Bexarotene blocks calcium-permeable ion channels formed by neurotoxic Alzheimer's beta-amyloid peptides. *ACS Chem Neurosci* **5**, 216–224.
- 27 Fantini J, Carls D & Yahi N (2011) The fusogenic tilted peptide (67–78) of  $\alpha$ -synuclein is a cholesterol binding domain. *Biochim Biophys Acta Biomembr* **1808**, 2343–2351.
- 28 O'Leary EI, Jiang Z, Strub M-P, Lee JC, O'Leary EI, Jiang Z, Strub M-P & Lee JC (2018) Effects of phosphatidylcholine membrane fluidity on the conformation and aggregation of N-terminally acetylated  $\alpha$ -synuclein. *J Biol Chem* **293**, 11195–11205.
- 29 Shvadchak VV, Falomir-Lockhart LJ, Yushchenko DA & Jovin TM (2011) Specificity and kinetics of alpha-synuclein binding to model membranes determined with fluorescent excited state intramolecular proton transfer (ESIPT) probe. *J Biol Chem* **286**, 13023–13032.
- 30 Sezgin E & Schwille P (2012) Model membrane platforms to study protein-membrane interactions. *Mol Membr Biol* **29**, 144–154.
- 31 Borch J & Hamann T (2009) The nanodisc: a novel tool for membrane protein studies. *Biol Chem* **390**, 805–814.
- 32 Dörr JM, Koorengel MC, Schäfer M, Prokofyev AV, Scheidelaar S, van der Cruijssen EAW, Dafforn TR, Baldus M & Killian JA (2014) Detergent-free isolation, characterization, and functional reconstitution of a tetrameric K<sup>+</sup> channel: the power of native nanodiscs. *Proc Natl Acad Sci USA* **111**, 18607–18612.
- 33 Denisov IG, Grinkova YV, Lazarides AA & Sligar SG (2004) Directed self-assembly of monodisperse phospholipid bilayer nanodiscs with controlled size. *J Am Chem Soc* **126**, 3477–3487.
- 34 Shortridge MD, Hage DS, Harbison GS & Powers R (2009) Estimating protein-ligand binding affinity using high-throughput screening by NMR. *J Comb Chem* **10**, 948–958.
- 35 Leung CWT, Guo F, Hong Y, Zhao E, Kwok RTK, Leung NLC, Chen S, Vaikath NN, El-Agnaf OM, Tang Y *et al.* (2015) Detection of oligomers and fibrils of  $\alpha$ -synuclein by AIEgen with strong fluorescence. *Chem Commun* **51**, 1866–1869.
- 36 Grey M, Linse S, Nilsson H, Brundin P & Sparr E (2011) Membrane interaction of  $\alpha$ -synuclein in different aggregation states. *J Parkinsons Dis* **1**, 359–371.
- 37 Pirc K & Ulrih NP (2015)  $\alpha$ -Synuclein interactions with phospholipid model membranes: key roles for electrostatic interactions and lipid-bilayer structure. *Biochim Biophys Acta Biomembr* **1848**, 2002–2012.
- 38 Nuscher B, Kamp F, Mehnert T, Odoy S, Haass C, Kahle PJ & Beyer K (2004)  $\alpha$ -synuclein has a high affinity for packing defects in a bilayer membrane: a thermodynamics study. *J Biol Chem* **279**, 21966–21975.
- 39 Rhoades E, Ramlall TF, Webb WW & Eliezer D (2006) Quantification of  $\alpha$ -synuclein binding to lipid vesicles using fluorescence correlation spectroscopy. *Biophys J* **90**, 4692–4700.
- 40 Zuidam NJ, Gouw HKME, Barenholz Y & Crommelin DJA (1995) Physical (in) stability of liposomes upon chemical hydrolysis: the role of lysophospholipids and fatty acids. *Biochim Biophys Acta Biomembr* **1240**, 101–110.
- 41 Halskau O, Froystein NA, Muga A & Martinez A (2002) The membrane-bound conformation of alpha-lactalbumin studied by NMR-monitored 1H exchange. *J Mol Biol* **321**, 99–110.
- 42 Harris FM, Best KB & Bell JD (2002) Use of laurdan fluorescence intensity and polarization to distinguish



- between changes in membrane fluidity and phospholipid order. *Biochim Biophys Acta Biomembr* **1565**, 123–128.
- 43 Antollini SS & Barrantes FJ (1998) Disclosure of discrete sites for phospholipid and sterols at the protein – lipid interface in native acetylcholine receptor-rich membrane. *Biochemistry* **37**, 16653–16662.
- 44 Parasassi T, De Stasio G, Ravagnan G, Rusch RM & Gratton E (1991) Quantitation of lipid phases in phospholipid vesicles by the generalized polarization of Laurdan fluorescence. *Biophys J* **60**, 179–189.
- 45 Parasassi T, Di Stefano M, Loiero M, Ravagnan G & Gratton E (1994) Influence of cholesterol on phospholipid bilayers phase domains as detected by Laurdan fluorescence. *Biophys J* **66**, 120–132.
- 46 Bagatoll LA, Parasassi T, Fidelio GD & Gratton E (1999) A model for the interaction of 6-Lauroyl-2-(N, N-dimethylamino)naphthalene with lipid environments: implications for spectral properties. *Photochem Photobiol* **70**, 557–564.
- 47 Fiorini R, Ventrella V, Trombetti F, Fabbri M, Pagliarani A & Nesci S (2019) Lipid-protein interactions in mitochondrial membranes from bivalve mollusks: molecular strategies in different species. *Comp Biochem Physiol B Biochem Mol Biol* **227**, 12–20.
- 48 Biancalana M & Koide S (2010) Molecular mechanism of Thioflavin-T binding to amyloid fibrils. *Biochim Biophys Acta Proteins Proteom* **1804**, 1405–1412.
- 49 Amdursky N, Erez Y & Huppert D (2012) Molecular rotors: what lies behind the high sensitivity of the thioflavin-T fluorescent marker. *Acc Chem Res* **45**, 1548–1557.
- 50 Meisl G, Kirkegaard JB, Arosio P, Michaels TCT, Vendruscolo M, Dobson CM, Linse S & Knowles TPJ (2016) Molecular mechanisms of protein aggregation from global fitting of kinetic models. *Nat Protoc* **11**, 252–272.
- 51 Voropai ES, Samtsov MP, Kaplevskii KN, Maskevich AA, Stepuro VI, Povarova OI, Kuznetsova IM, Turoverov KK, Fink AL & Uverskii VN (2003) Spectral properties of thioflavin T and its complexes with amyloid fibrils. *J Appl Spectrosc* **70**, 868–874.
- 52 Afitska K, Fucikova A, Shvadchak VV & Yushchenko DA (2017) Modification of C terminus provides new insights into the mechanism of  $\alpha$ -Synuclein aggregation. *Biophys J* **113**, 2182–2191.
- 53 Morris AM, Watzky MA, Agar JN & Finke RG (2008) Fitting neurological protein aggregation kinetic data via a 2-step, minimal/"Ockham's razor" model: the Finke-Watzky mechanism of nucleation followed by autocatalytic surface growth. *Biochemistry* **47**, 2413–2427.
- 54 Bermel W, Bertini I, Felli IC, Lee YM, Luchinat C & Pierattelli R (2006) Protonless NMR experiments for sequence-specific assignment of backbone nuclei in unfolded proteins. *J Am Chem Soc* **128**, 3918–3919.
- 55 Porcari R, Proukakis C, Waudby CA, Bolognesi B, Mangione PP, Paton JFS, Mullin S, Cabrita LD, Penco A, Relini A *et al.* (2015) The H50Q mutation induces a 10-fold decrease in the solubility of  $\alpha$ -synuclein. *J Biol Chem* **290**, 2395–2404.
- 56 Fusco G, De Simone A, Gopinath T, Vostrikov V, Vendruscolo M, Dobson CM & Veglia G (2014) Direct observation of the three regions in  $\alpha$ -synuclein that determine its membrane-bound behaviour. *Nat Commun* **5**, 3827.
- 57 Liang B & Tamm LK (2018) Solution NMR of SNAREs, complexin and  $\alpha$ -synuclein in association with membrane-mimetics. *Prog Nucl Magn Reson Spectrosc* **105**, 41–53.
- 58 Terakawa MS, Lee Y-H, Kinoshita M, Lin Y, Sugiki T, Fukui N, Ikenoue T, Kawata Y & Goto Y (2018) Membrane-induced initial structure of  $\alpha$ -synuclein control its amyloidogenesis on model membranes. *Biochim Biophys Acta Biomembr* **1860**, 757–766.
- 59 Niklasson M, Otten R, Ahlner A, Andresen C, Schlagnitweit J, Petzold K & Lundström P (2017) Comprehensive analysis of NMR data using advanced line shape fitting. *J Biomol NMR* **69**, 93–99.
- 60 Davidson WS, Jonas A, Clayton DF & George JM (1998) Stabilization of  $\alpha$ -Synuclein secondary structure upon binding to synthetic membranes. *J Biol Chem* **273**, 9443–9449.
- 61 Eliezer D, Kutluay E, Bussell R & Browne G (2001) Conformational properties of alpha-synuclein in its free and lipid-associated states. *J Mol Biol* **307**, 1061–1073.
- 62 Beyer K (2007) Mechanistic aspects of Parkinson's disease:  $\alpha$ -synuclein and the biomembrane. *Cell Biochem Biophys* **47**, 285–299.
- 63 Fantini J & Yahi N (2010) Molecular insights into amyloid regulation by membrane cholesterol and sphingolipids: common mechanisms in neurodegenerative diseases. *Expert Rev Mol Med* **12**, 1–22.
- 64 Lautenschläger J, Stephens AD, Fusco G, Ströhl F, Curry N, Zacharopoulou M, Michel CH, Laine R, Nespovitaya N, Fantham M *et al.* (2018) C-terminal calcium binding of  $\alpha$ -synuclein modulates synaptic vesicle interaction. *Nat Commun* **9**, 712.
- 65 Terakawa MS, Lin Y, Kinoshita M, Kanemura S, Itoh D, Sugiki T, Okumura M, Ramamoorthy A & Lee YH (2018) Impact of membrane curvature on amyloid aggregation. *Biochim Biophys Acta Biomembr* **1860**, 1741–1764.
- 66 Aliakbari F, Mohammad-Beigi H, Rezaei-Ghaleh N, Becker S, Dehghani Esmatabad F, Eslampanah Seyedi HA, Bardania H, Tayaranian Marvian A, Collingwood JF, Christiansen G *et al.* (2018) The potential of zwitterionic nanoliposomes against neurotoxic alpha-

- synuclein aggregates in Parkinson's Disease. *Nanoscale* **10**, 9174–9185.
- 67 Vorobyov I & Allen TW (2011) On the role of anionic lipids in charged protein interactions with membranes. *Biochim Biophys Acta Biomembr* **1808**, 1673–1683.
- 68 Yeung T, Gilbert GE, Shi J, Silvius J, Kapus A & Grinstein S (2008) Membrane phosphatidylserine regulates surface charge and protein localization. *Science* **319**, 210–213.
- 69 Stahelin RV, Scott JL & Frick CT (2014) Cellular and molecular interactions of phosphoinositides and peripheral proteins. *Chem Phys Lipids* **182**, 3–18.
- 70 Rødland I, Halskau Ø, Martínez A & Holmsen H (2005)  $\alpha$ -Lactalbumin binding and membrane integrity – effect of charge and degree of unsaturation of glycerophospholipids. *Biochim Biophys Acta Biomembr* **1717**, 11–20.
- 71 Stöckl M, Fischer P, Wanker E & Herrmann A (2008)  $\alpha$ -Synuclein selectively binds to anionic phospholipids embedded in liquid-disordered domains. *J Mol Biol* **375**, 1394–1404.
- 72 Galvagnion C, Brown JWP, Ouberai MM, Flagmeier P, Vendruscolo M, Buell AK, Sparr E & Dobson CM (2016) Chemical properties of lipids strongly affect the kinetics of the membrane-induced aggregation of  $\alpha$ -synuclein. *Proc Natl Acad Sci USA* **113**, 7065–7070.
- 73 Van Maarschalkerweerd A, Vetri V & Vestergaard B (2015) Cholesterol facilitates interactions between  $\alpha$ -synuclein oligomers and charge-neutral membranes. *FEBS Lett* **589**, 2661–2667.
- 74 Nyholm TKM, Lindroos D, Westerlund B & Slotte JP (2011) Construction of a DOPC/PSM/cholesterol phase diagram based on the fluorescence properties of trans -parinaric acid. *Langmuir* **27**, 8339–8350.
- 75 Marsh D (2009) Cholesterol-induced fluid membrane domains: a compendium of lipid-raft ternary phase diagrams. *Biochim Biophys Acta Biomembr* **1788**, 2114–2123.
- 76 Blosser MC, Starr JB, Turtle CW, Ashcraft J & Keller SL (2013) Minimal effect of lipid charge on membrane miscibility phase behavior in three ternary systems. *Biophys J* **104**, 2629–2638.
- 77 Gentry KA, Prade E, Barnaba C, Zhang M, Mahajan M, Im S-C, Anantharamaiah GM, Nagao S, Waskell L & Ramamoorthy A (2017) Kinetic and structural characterization of the effects of membrane on the complex of cytochrome b 5 and cytochrome c. *Sci Rep* **7**, 1–15.
- 78 Bosco DA, Fowler DM, Zhang Q, Nieva J, Powers ET, Wentworth P, Lerner RA & Kelly JW (2006) Elevated levels of oxidized cholesterol metabolites in Lewy body disease brains accelerate  $\alpha$ -synuclein fibrilization. *Nat Chem Biol* **2**, 249–253.
- 79 Bar-On P, Crews L, Koob AO, Mizuno H, Adame A, Spencer B & Masliah E (2008) Statins reduce neuronal  $\alpha$ -synuclein aggregation in in vitro models of Parkinson's disease. *J Neurochem* **105**, 1656–1667.
- 80 Peng C, Gathagan RJ, Covell DJ, Medellin C, Stieber A, Robinson JL, Zhang B, Pitkin RM, Olufemi MF, Luk KC *et al.* (2018) Cellular milieu imparts distinct pathological  $\alpha$ -synuclein strains in  $\alpha$ -synucleinopathies. *Nature* **557**, 558–563.
- 81 George JM, Jin H, Woods WS & Clayton DF (1995) Characterization of a novel protein regulated during the critical period for song learning in the zebra finch. *Neuron* **15**, 361–372.
- 82 Bussell R & Eliezer D (2003) A structural and functional role for 11-mer repeats in  $\alpha$ -synuclein and other exchangeable lipid binding proteins. *J Mol Biol* **329**, 763–778.
- 83 Rodriguez JA, Ivanova MI, Sawaya MR, Cascio D, Reyes FE, Shi D, Sangwan S, Guenther EL, Johnson LM, Zhang M *et al.* (2015) Structure of the toxic core of  $\alpha$ -synuclein from invisible crystals. *Nature* **525**, 486–490.
- 84 Kim TD, Paik SR & Yang CH (2002) Structural and functional implications of C-terminal regions of alpha-synuclein. *Biochemistry* **41**, 13782–13790.
- 85 Li W, West N, Colla E, Pletnikova O, Troncoso JC, Marsh L, Dawson TM, Jakala P, Hartmann T, Price DL *et al.* (2005) Aggregation promoting C-terminal truncation of alpha-synuclein is a normal cellular process and is enhanced by the familial Parkinson's disease-linked mutations. *Proc Natl Acad Sci USA* **102**, 2162–2167.
- 86 Wennberg CL, Van Der Spoel D & Hub JS (2012) Large influence of cholesterol on solute partitioning into lipid membranes. *J Am Chem Soc* **134**, 5351–5361.
- 87 Alwarawrah M, Dai J & Huang J (2010) A molecular view of the cholesterol condensing effect in DOPC lipid bilayers. *J Phys Chem B* **114**, 7516–7523.
- 88 Berg D, Riess O & Bornemann A (2003) Specification of 14-3-3 proteins in Lewy bodies. *Ann Neurol* **54**, 135.
- 89 Wakabayashi K, Umahara T, Hirokawa K, Hanyu H & Uchiyama T (2018) 14-3-3 protein sigma isoform co-localizes with phosphorylated  $\alpha$ -synuclein in Lewy bodies and Lewy neurites in patients with Lewy body disease. *Neurosci Lett* **674**, 171–175.
- 90 Martin H, Rostas J, Patel Y & Aitken A (2002) Subcellular localisation of 14-3-3 isoforms in rat brain using specific antibodies. *J Neurochem* **63**, 2259–2265.
- 91 Plotegher N, Kumar D, Tessari I, Brucale M, Munari F, Tosatto L, Belluzzi E, Greggio E, Bisaglia M, Capaldi S *et al.* (2014) The chaperone-like protein 14-3-3h interacts with human  $\alpha$ -synuclein aggregation intermediates rerouting the amyloidogenic pathway and reducing  $\alpha$ -synuclein cellular toxicity. *Hum Mol Genet* **23**, 5615–5629.
- 92 Caldinelli L, Albani D & Pollegioni L (2013) One single method to produce native and Tat-fused recombinant

- human alpha-synuclein in *Escherichia coli*. *BMC Biotechnol* **13**, 1–8.
- 93 van den Berg S, Lofdahl PA, Hard T & Berglund H (2006) Improved solubility of TEV protease by directed evolution. *J Biotechnol* **121**, 291–298.
- 94 Marley J, Lu M & Bracken C (2001) A method for efficient isotopic labeling of recombinant proteins. *J Biomol NMR* **20**, 71–75.
- 95 Studier FW (2005) Protein production by auto-induction in high-density shaking cultures. *Protein Expr Purif* **41**, 207–234.
- 96 Torchilin V & Weissig V (2003) *Liposomes: A Practical Approach*. Oxford, UK: Oxford University Press.
- 97 Swainsbury DJK, Scheidelaar S, van Grondelle R, Killian JA & Jones MR (2014) Bacterial reaction centers purified with styrene maleic acid copolymer retain native membrane functional properties and display enhanced stability. *Angew Chem Int Ed* **53**, 11803–11807.
- 98 Scheidelaar S, Koorengel MC, Pardo JD, Meeldijk JD, Breukink E & Killian JA (2015) Molecular model for the solubilization of membranes into nanodisks by styrene maleic acid copolymers. *Biophys J* **108**, 279–290.
- 99 Ahlner A, Carlsson M, Jonsson BH & Lundström P (2013) PINT: a software for integration of peak

volumes and extraction of relaxation rates. *J Biomol NMR* **56**, 191–202.

## Supporting information

Additional supporting information may be found online in the Supporting Information section at the end of the article.

**Fig. S1.** Nanodiscs preparation.

**Fig. S2.** Generalized polarization for both lipid nanodiscs and lipid vesicles.

**Fig. S3.** LC-MS/MS analysis of nanodiscs for the presence of cholesterol.

**Fig. S4.** Monomeric  $\alpha$ -Syn.

**Fig. S5.** TPE-TPP fluorescence is inhibited by the presence of lipids.

**Table S1.** Table of lipid nanodiscs used throughout the study.

**Table S2.** Zeta potential measurement of lipid nanodiscs and vesicles of same lipid composition.

**Table S3.** Primers used for site-directed mutagenesis.

**Table S4.** Residue-specific  $aK_D$  values.

**Appendix S1.** Cholesterol-containing lipid nanodiscs promote  $\alpha$ -Synuclein oligomerization.